Arabian Journal for Science and Engineering
https://doi.org/10.1007/s13369-023-08576-0

RESEARCH ARTICLE-CHEMICAL ENGINEERING

# Cost-Effective Single-Step Synthesis of Metal Oxide-Supported Ni Catalyst for $H_2$-Production Through Dry Reforming of Methane

**Ahmed S. Al-Fatesh[1] · Nouf A. Bamatraf[2] · Salwa B. Alreshaidan[2] · Jehad K. Abu-Dahrieh[3] · Naitik patel[4] · Ahmed A. Ibrahim[1] · Anis H. Fakeeha[1] · Abdulrahman bin Jumah[1] · Rawesh Kumar[4]**

Received: 3 May 2023 / Accepted: 27 November 2023


**Abstract**

Preparing catalysts from cheap metal precursors in a single pot are an appealing method for reducing catalytic preparation costs, minimizing chemical waste, and saving time. With regards to the catalytic conversion of dry reforming of methane, it offers the prospect of significantly reducing the cost of $H_2$ production. Herein, NiO-stabilized metal oxides like Ni/$TiO_2$, Ni/MgO, Ni/$ZrO_2$, and Ni/$Al_2O_3$ are prepared at two different calcination temperatures (600 °C and 800 °C). Catalysts are characterized by X-ray diffraction, Raman spectroscopy, surface area-porosity analysis, Temperature program experiments, infrared spectroscopy, and thermogravimetry analysis. The MgO-supported Ni catalyst (Ni/MgO-600), $ZrO_2$-supported Ni catalyst (Ni/$ZrO_2$-600), and $Al_2O_3$-supported Ni (Ni/$Al_2O_3$-600) catalyst calcined at 600 °C show initial equal $H_2$ yields (~ 55%). The population of $CH_4$ decomposition sites over $ZrO_2$-supported Ni catalyst remains highest, but $H_2$-yield drops to 45% against high coke deposition. The catalytic activity remains constant over the Ni/MgO-600 catalyst due to the enrichment of "surface interacted $CO_2$-species". MgO-supported Ni catalyst calcined at 800 °C undergoes weak interactions of NiO-M′ (M′ = support), serious loss of $CH_4$ decomposition sites and potential consumption of $H_2$ by reverse water gas shift reaction, resulting in inferior $H_2$ yield. $H_2$-yield remains unaffected over an $Al_2O_3$-supported Ni catalyst even against the highest coke deposition due to the formation of stable Ni (which exsolves from $NiAl_2O_4$) and proper matching between carbon formation and rate of carbon diffusion.

**Keywords** $TiO_2$ · MgO · $Al_2O_3$ · $ZrO_2$ · Supported Ni catalyst · Dry reforming of methane

## 1 Introduction

The enormous addition of greenhouse gases to the environment brings global warming and climatic disbalance worldwide. In this run, catalytic conversion of greenhouse gases like $CH_4$ and $CO_2$ into hydrogen-rich syngas up to the industrial scale may be a potential hope. This reaction is popularly known as the dry reforming of methane (DRM), and it is operated at highly endothermic conditions ($CH_4 + CO_2 \rightarrow 2H_2 + 2CO$; $\Delta H = 247$ kJ/mol). $H_2$ is not only a green energy source, but also it has three times more energy content than gasoline [1]. The commercial production of $H_2$ through DRM reaction may fulfill energy demand and amend the environment by depleting the concentration of greenhouse gases ($CH_4$ and $CO_2$). The DRM community worked vigorously toward high-performance catalytic development by modifying preparation conditions, choosing active metal precursors, selecting support, and optimizing loading by promoters. Using a promoter-based catalyst system generally

✉ Jehad K. Abu-Dahrieh
j.abudahrieh@qub.ac.uk

Ahmed S. Al-Fatesh
aalfatesh@ksu.edu.sa

Rawesh Kumar
kr.rawesh@gmail.com

1 Chemical Engineering Department, College of Engineering, King Saud University, P.O. Box 800, 11421 Riyadh, Saudi Arabia

2 Department of Chemistry, Faculty of Science, King Saud University, P.O. Box 800, 11451 Riyadh, Saudi Arabia

3 School of Chemistry and Chemical Engineering, Queen's University Belfast, Belfast BT9 5AG, Northern Ireland, UK

4 Department of Chemistry, Indus University, Ahmedabad, Gujarat 382115, India

Published online: 23 January 2024

requires more steps for synthesis, and after optimum loading, it may also shade the catalytic active sites. It raises the synthetic cost of the catalyst also. So, handy catalyst preparation relies more on metal precursors and support and excludes the use of promoters.

Novel metals and Ni are catalytic active sites for DRM, and the dispersion of catalytic active sites for potential conversion needs support. The DRM reaction is operated at a very high reaction temperature and retaining stable catalytic active sites at this temperature are even more challenging. The size and morphology of Ni can be controlled by proper calcination methodology and mixing a suitable matrix with Ni during catalyst preparation [2, 3]. Dispersion of cheap active metals like Ni (derived from cheap metal precursors) over thermally sustainable metal oxide supports like titania, magnesium oxide, alumina, and zirconia by simple synthetic pathways may be an option for preparing handy and cheap catalyst. Among different alkaline earth metal oxides, MgO-support has adequate basicity, high thermal sustainability, and high thermal conductivity [4]. So, it is readily used as a basic ceramic material. MgO-supported Ni catalyst was found promising at intermediate calcination temperatures (600 °C) due to the complete formation of NiO-MgO solid solutions [5]. However, a higher calcination temperature (700 °C) resulted in the formation of a larger Ni size, a harder framework, lower reducibility, and lower catalytic activity toward DRM. Again, high-pre-treatment temperatures (800 °C) also dictated severe sintering of metallic Ni, high-coke deposition, and lower catalytic activity [6].

A Titania-supported Ni catalyst can be used as a photocatalyst and a thermal catalyst for the DRM reaction [7, 8]. The phase transition of $TiO_2$ support and partial coverage of active Ni sites by $TiO_x$ species were major drawbacks in achieving higher activity toward DRM [7, 9]. Zhang et al. conducted a $CH_4$-temperature programmed surface reaction without oxidizing agents ($O_2$/$CO_2$) over Ni/$ZrO_2$. Still, they detected CO. It indicates the involvement of lattice oxygen in the $ZrO_2$ lattice during $CH_4$ oxidation [10]. Instant involvement of lattice oxygen for carbon deposit oxidation, creating a vacancy behind, and after that, oxygen replenishment of oxygen by $CO_2$ is a terrific pathway to minimize the delay in the $CH_4$ oxidation reaction [11]. The oxygen-endowing capacity of $ZrO_2$ (from its lattice) makes it superior to $Al_2O_3$. NiO-$ZrO_2$ solid solution was claimed for consistent catalytic activity toward DRM [12–14]. Ni-impregnated $ZrO_2$ showed about 43–46% $H_2$-yield [11, 15]. However, phase transition at higher temperatures limited the activity toward DRM.

Alumina is widely available in the earth's crust and is known for its high thermal sustainability and high thermal conductivity, hardness, and passiveness to the atmosphere. Alumina is an excellent carrier for stabilizing Ni at high temperatures. At high temperatures up to 900 °C, NiO is diffused into the $Al_2O_3$ support, coordinates with Al (tetrahedrally and octahedrally), and generates reducible $NiAl_2O_4$ species [16–18]. During reductive pre-treatment of the catalyst (before the DRM reaction), Ni derived from $NiAl_2O_4$ was found to have stable active sites for $CH_4$ decomposition in the DRM reaction. Al-Fatesh et al. showed an increase in basicity (or $CO_2$ absorption) at a higher pre-treatment temperature (800 °C), whereas Bian et al. showed the same at a higher calcination temperature (700 °C) [19, 20]. He et al. [21] showed increased metal-support interaction and high Ni dispersion on increasing calcination temperature. Qiu et al. [22] optimized the best performance of an alumina-supported Ni catalyst at 600 °C calcination temperature and 700 °C reduction temperature. The preparation method is also crucial for high catalytic activity. 23% $H_2$ yield was noticed over Ni impregnated over $Al_2O_3$, whereas 58% $H_2$-yield is claimed over Ni/$Al_2O_3$ prepared by microwave-assisted combustion synthesis [23].

The supported metal catalysts are synthesized in multiple pots and single pot. Preparation of supports by hydrothermal/sol–gel followed by impregnation of active metal over a support needs multiple pots during synthesis [24, 25]. It leads to chemical wastage and longer time duration. The one-pot synthetic strategy minimizes chemical waste and saves time as the entire synthesis is carried out in a single pot. Herein, dispersion of cheap active metals, like Ni (derived from cheap metal precursors), over different metal oxides carriers like titania, magnesium oxides, alumina, and zirconia are carried out in a single pot at two different calcination temperatures (600 °C and 800 °C). The catalyst samples are investigated for dry reforming of methane and characterized by X-ray diffraction (XRD), Raman spectroscopy, Infrared spectroscopy, surface area and porosity, $H_2$-Temperature programmed reduction ($H_2$-TPR), $CH_4$-temperature programmed surface reaction ($CH_4$-TPSR), $CO_2$-temperature programmed desorption ($CO_2$-TPD) and thermogravimetry. The physiochemical changes over the catalyst surface during calcination temperature vis-à-vis their effect on catalytic activity is a guide for developing a handy, single-step synthesis, promoter-free, metal oxide-supported Ni catalyst for DRM.

## 2 Experimental

### 2.1 Materials

Ni $(NO_3)_2.6H_2O$ (98%, Alfa Aesar), titania ($TiO_2$-P25, 99.9%, from Degussa p25, Nanoshel, Cheshire, UK), alumina ($Al_2O_3$, 97.7% Norton Chemical Process Products Corp), magnesia (MgO, 99.5%. BDH), and zirconia (ZrO2, 99.8%, Anhui-Elite, China).

### 2.2 Catalyst Preparation

The nickel nitrate precursor salt solution (equivalent to 5 wt%) is added over a support (like $TiO_2$, $Al_2O_3$, MgO, and $ZrO_2$) under stirring and heating until all water is evaporated. The paste is dried at 110 °C. One set of dry catalysts is calcined at 600 °C for 3 h (at 3 °C/min heating ramp), and another set of dry catalysts is calcined at 800 °C for 3 h. The catalysts calcined at 600 °C are abbreviated as Ni/$TiO_2$-600, Ni/$Al_2O_3$-600, Ni/MgO-600, Ni/$ZrO_2$-600 whereas catalyst calcined at 800 °C are abbreviated as Ni/$TiO_2$-800, Ni/$Al_2O_3$-800, Ni/MgO-800, Ni/$ZrO_2$-800.

Accordingly, the 5.0 wt% NiO supported over S (S = $TiO_2$, $Al_2O_3$, MgO, or $ZrO_2$) catalysts were produced by dissolving 0.5 g of Ni $(NO_3)_2{\cdot}6H_2O$ in 30 ml of distilled water with stirring and heating. Afterward, 2.441 g of support was added, and the stirring was continued for 30 min. The obtained catalysts were dehydrated at 120°C for 20 h and were then calcined for five hours either at 600 °C or 800 °C.

### 2.3 Catalyst Characterization

The surface area and porosity of the catalyst samples were studied using the Brunauer–Emmet–Teller (BET) method and the Barrett–Joyner–Halenda (BJH) method on a Micromeritics Trostat II 3020. X-ray diffraction (XRD) study and phase analysis of catalyst samples were carried out over a Miniflex Rigaku diffractometer using the Cu Kα radiation source (at 40 kV and 40 mA) and the JCPDS database, respectively. Laser Raman spectra of catalysts are taken by the JASCO NMR-4500 spectrometer in the spectral range of 170–1000 $cm^{-1}$ by using a 532 nm excitation wavelength and 1.6 mW laser power for 10 s of exposure time at 3 accumulations. Spectra were processed using Spectra Manager Ver. 2 software (JASCO, Japan). The electronic transition study was conducted under 1 nm resolution in the 200–1000 nm range at 200 nm/min scanning speed over a V-570 (JASCO, USA) ultraviolet–visible spectrophotometer. The $H_2$-Temperature programmed reduction profile is analyzed over a 70 mg sample under 10% $H_2$/Ar gas flow (flow rate 30 ml/min) up to 900 °C temperature (heating ramp 10 °C/min) in the Micromeritics Auto Chem II 2920 USA instrument. For $CH_4$-temperature programmed surface reaction, the same procedure is followed with 10% $CH_4$/Ar mixture (in place of 10%$H_2$/Ar mixture). The $CH_4$ or $H_2$ consumption amount is determined by the thermal conductivity detector (TCD). For $CO_2$-temperature programmed desorption, 70 mg of the sample was kept at 200 °C for 1 h under helium flow (to remove physically adsorbed species) and then subjected to a 10% $CO_2$/He mixture (flow rate of 30 ml/min) at 50 °C for 30 min. Then, the $CO_2$ desorption signal was recorded by TCD with a linear increase in temperature up to 1000 °C with a temperature ramp rate of 10 °C/min. Fourier transforms infrared spectra of catalyst samples are recorded over the KBr pallet in 400–4000 $cm^{-1}$ range using Prestige-21 SHIMADZU. Ultraviolet–visible spectra of catalyst samples are recorded in 200–800 nm range at a resolution of 1 nm (200 nm/min scanning speed) using the V-570, JASCO (USA). The weight loss % of the spent catalyst sample (15 mg) was determined by thermogravimetry analysis under oxidative treatment from room temperature to 1000 °C (20 °C/min heating ramp) using Shimadzu TGA-51.

### 2.4 Catalyst Activity Test

0.1 g of catalyst is packed in a tubular stainless-steel reactor (PID Eng & Tech micro-activity reference company, length 30 cm, internal diameter 9.1 mm). An axially injected K-type thermocouple monitors the catalyst bed temperature. The packed catalyst is activated under $H_2$ flow (flow rate 30 ml/min) at 700 °C for 1 h. Further, $CH_4$, $CO_2$, and $N_2$ gas feed (feed ratio 3:3:1) are passed through a packed activated catalyst with a 42,000 ml/h gcat space velocity at 700 °C reaction temperature. The effluent is examined under Ar carrier gas by gas chromatograph instrument equipped with molecular sieve 5 A column, Porapak Q column, and TCD detector. $H_2$ yield % and CO yield % are determined by the following expressions:

$$H_2\text{Yield}\% = \frac{\left(n_{H_2}\right)_{out}}{2 \times \left(n_{CH_4}\right)_{in}} \times 100$$

$$\text{CO Yield}\% = \frac{(n_{CO})_{out}}{\left(n_{CH_4}\right)_{in} + \left(n_{CO_2}\right)_{in}} \times 100$$

where $\left(n_{H_2}\right)_{out}$ is Mole of $H_2$ in product (outlet), $\left(n_{CH_4}\right)_{in}$ is mole of $CH_4$ in inlet, $(n_{CO})_{out}$ is mole of CO in product (outlet), and $(n_{CO})_{in}$ is mole of $CO_2$ in inlet.

## 3 Result

### 3.1 Characterization Result

Figure S1 displays the catalyst sample's X-ray diffraction pattern. After calcining Titania supported Ni calcined at 600 °C, both rutile $TiO_2$ phase (JCPDS reference number 00–021-1272) and anatase $TiO_2$ phase (JCPDS reference number 01–076-0334) are organized in the catalyst. (Fig. S1a). Upon higher calcination temperature (800 °C), rutile phase is stable. The effect of calcination temperature is not evident on the phase distribution of $Al_2O_3$-supported Ni, $ZrO_2$-supported Ni and MgO-supported Ni catalysts (Fig. S1b–d). Alumina-supported Ni catalyst exhibited cubic phases of nickel aluminum oxide (JCPDS reference number 00-001-1299), aluminum oxide (JCPDS reference number

00-004-0858) and nickel oxide (JCPDS reference number 01-071-1179). MgO-supported Ni catalyst has both cubic magnesium nickel oxide phase (JCPDS reference number 00-034-0410) and cubic magnesium oxide (JCPDS reference number 00-043-1022), while the $ZrO_2$-supported Ni catalyst contains only monoclinic phase (JCPDS reference number 00-024-1165).

The Raman spectra of catalyst samples are shown in Fig. 1. Titania-supported Ni catalyst calcined at 600 °C shows a prominent Raman band for the anatase phase at 399 $cm^{-1}$ ($B_{1g}$), 511 $cm^{-1}$ ($A_{1g}$) 518 $cm^{-1}$ ($B_{1g}$) and 639 $cm^{-1}$ ($E_g$) and a diffuse Raman band for the rutile phase at 447 $cm^{-1}$ ($E_g$) [26] (Fig. 1a). Interestingly, if the same catalyst is prepared at 800 °C calcination temperature, the three peaks disappear over Ni/$TiO_2$-800 catalyst and high-intensity peaks related to rutile phases at 242 $cm^{-1}$, 447 $cm^{-1}$ ($E_g$), 612 $cm^{-1}$ ($A_{1g}$) appear [26, 27]. It indicates the phase transition of titania from anatase to rutile phases from 600 °C to 800 °C calcination temperature. Zirconia-supported Ni catalysts (Ni/$ZrO_2$-600 and Ni/$ZrO_2$-800) showed high-intensity peaks of monoclinic zirconia at 179 $cm^{-1}$, 188 $cm^{-1}$, 220 $cm^{-1}$, 301 $cm^{-1}$, 333 $cm^{-1}$, 342 $cm^{-1}$, 379 $cm^{-1}$, 476 $cm^{-1}$, 536 $cm^{-1}$, 559 $cm^{-1}$ and 610 $cm^{-1}$ and 636 $cm^{-1}$ [28–30] (Fig. 1b). The catalyst calcined at higher temperature (Ni/$ZrO_2$-800) has high-intensity peaks of monoclinic zirconia. The Raman spectroscopy results of titania-supported Ni and zirconia-supported Ni catalysts are found in the same line as X-ray diffraction results. MgO-supported Ni catalyst and $Al_2O_3$-supported Ni catalysts were found to be Raman inactive (Fig. S2).

The $N_2$-adsorption isotherm and surface parameters (surface area, pore volume and average pore diameter) of catalyst samples are shown in Fig. 2. The surface area catalyst samples calcined at 600 °C are found in the following order: Ni/$Al_2O_3$-600 > Ni/MgO-600 > Ni/$TiO_2$-600 > Ni/$ZrO_2$-600. That means alumina-supported Ni catalyst has the highest surface area and pore volume, whereas zirconia-supported Ni catalysts has the least surface area and pore volume at 600 °C calcination temperature. However, if catalyst samples are calcined at a higher calcination temperature of 800 °C, a sharp fall of the surface area is observed in $TiO_2$-supported Ni catalyst, and a noticeable fall of the surface area is marked for MgO-supported Ni catalysts, $ZrO_2$-supported Ni catalysts and $Al_2O_3$-supported Ni catalyst (Fig. 2e). It is again markable that the average pore diameter of "high temperature calcined catalyst" is larger than "low-temperature calcined catalyst". It indicates conversion of smaller pores into large pores upon higher calcination temperature. Overall, the fall in surface area and nurture of larger pore diameter upon higher calcination temperature signifies for substantial pore damage (or collapse of the small pores to form the big ones) [31–33]. Even though the surface area and pore diameter of $Al_2O_3$-supported Ni catalyst calcined at 800 °C remain highest in its series. That means, the $Al_2O_3$-supported Ni catalyst is almost unaffected by calcination temperature.

The $H_2$-temperature programmed reduction profile of different catalysts is shown in Fig. 3. The reduction peaks at different temperatures indicate the extent of reduction of different "surface interacted NiO species". The reduction peaks below 500 °C, 500–700 °C, and 700–1000 °C are attributed to the reduction of NiO species that interacted weakly, moderately, and strongly with the support, respectively [17]. Titania-supported Ni catalysts have reducible NiO species that interact moderately with support, whereas alumina-supported Ni catalysts have reducible NiO species that strongly interacts with support (Fig. 3a, b). Over an alumina-supported Ni catalyst, some Ni ions may be diffused into the $Al_2O_3$ support at high temperatures and form stable $NiAl_2O_4$. The $NiAl_2O_4$-species is reducible above 700 °C. The XRD pattern of the alumina-supported Ni catalyst also showed the presence of $NiAl_2O_4$ phases. Interestingly, in our case, the catalyst activation temperature is also set at 700 °C. That means, at this temperature, Ni exsolves from the stable $NiAl_2O_4$ phase and presents a stable catalytic active site for the DRM reaction. It is again noticeable that if titania-supported Ni catalyst or alumina-supported Ni catalyst are prepared by calcining at a high temperature (800 °C), the intensity of reduction peaks decreases and the pattern of reduction peaks shifts toward a relatively lower temperature. It indicates the increasing edge of reducibility for the catalyst calcined at high temperatures. MgO-supported Ni catalysts have a very poor reducibility profile (Fig. 3c). That means, it has very few reducible NiO species at the catalyst surface. Possibly due to the formation of stable cubic magnesium nickel oxide phases, reducible NiO species are depleted over the catalyst surface. The reducible profile of zirconia-supported Ni catalyst is unique (Fig. 3d). $ZrO_2$-supported Ni species calcined at 600 °C has two reduction peaks at about 350 °C and 550 °C indicating the presence of both "weakly and moderately interacted NiO-species" over the catalyst surface [34]. Interestingly, if the catalyst is prepared at a high-calcination temperature (800 °C), the peak intensity of weakly interacted NiO species is shifted toward a higher temperature, and an intense single peak about peak maxima 475 °C appears. That means, the catalyst calcined at 800 °C has a higher metal-support interaction with reducible "moderately interacted NiO-species".

Infrared transmittance spectra of catalyst samples are shown in Fig. 4. The infrared vibration peak of the metal–oxygen bond falls in the lower wavelength region (< 800 $cm^{-1}$) due to the high atomic weight of metal and the reduced mass of the metal–oxygen pair (compared to nonmetal-oxygen pairs such as OH, C-O) [35]. The Ni–O vibration peak for free NiO species was reported at 433 $cm^{-1}$ [36]. The IR vibration peak < 433 $cm^{-1}$ indicates the weakening of bond strength between Ni and O (Ni–O bond)

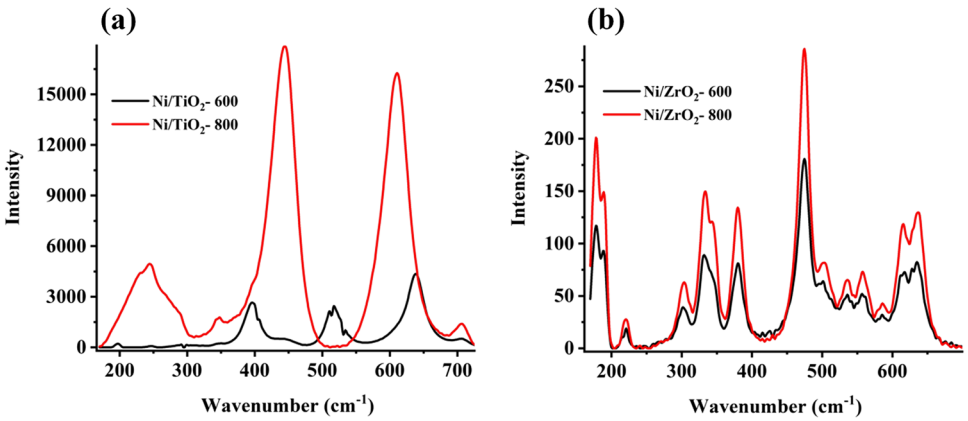


**Fig. 1** Raman spectra of (**a**) $Ni/TiO_2$-600 and $Ni/TiO_2$-800 (**b**) $Ni/ZrO_2$-600 and $Ni/ZrO_2$-800

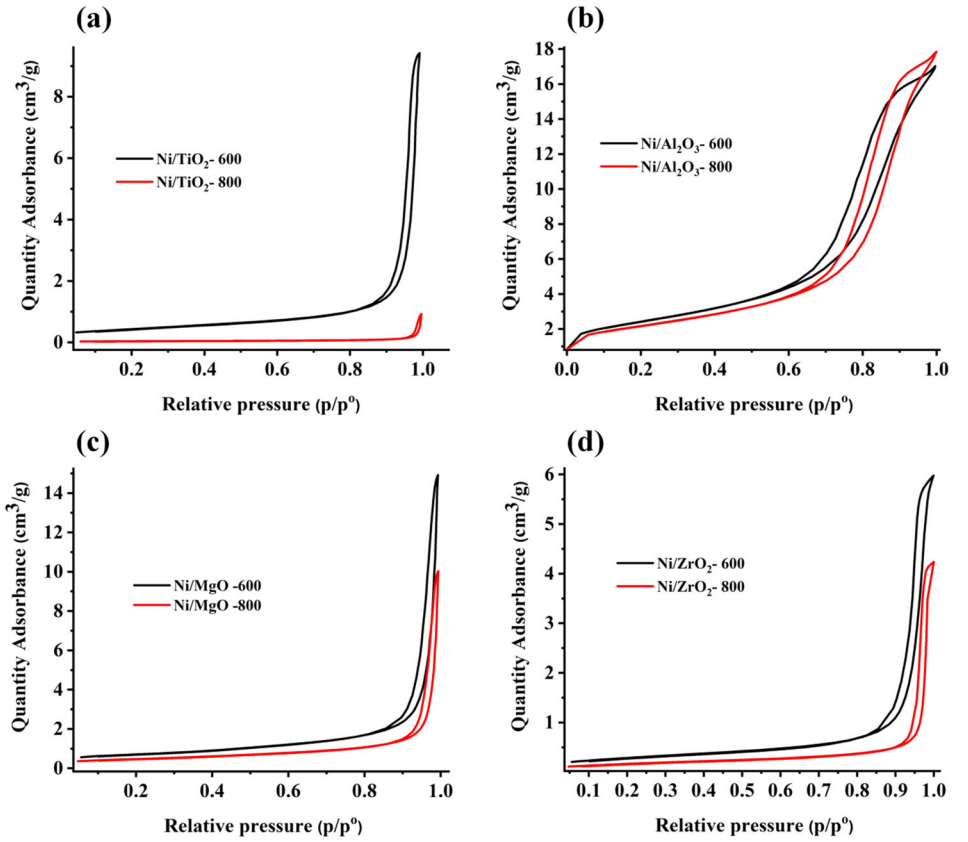


**Fig. 2** $N_2$-adsorption isotherm of catalysts (**a**) $Ni/TiO_2$-600 and $Ni/TiO_2$-800 (**b**) $Ni/Al_2O_3$-600 and $Ni/Al_2O_3$-800 (**c**) Ni/MgO-600 and Ni/MgO-800 (**d**) $Ni/ZrO_2$-600 and $Ni/ZrO_2$-800 (**e**) The surface area, pore volume and Average pore diameter of different catalysts.

(e)

| Catalyst | Surface Area ($m^2/g$) | Pore Volume ($cm^3/g$) | Average Pore Diameter (nm) |
|---|---|---|---|
| **$Ni/TiO_2$-600** | 34.77 | 0.33 | 36.7 |
| **$Ni/TiO_2$-800** | 3.04 | 0.032 | 51.2 |
| **Ni/MgO-600** | 55.20 | 0.52 | 35.4 |
| **Ni/MgO-800** | 37.12 | 0.35 | 40.0 |
| **$Ni/Al_2O_3$-600** | 196 | 0.61 | 9.71 |
| **$Ni/Al_2O_3$-800** | 175.29 | 0.67 | 11.2 |
| **$Ni/ZrO_2$-600** | 23.75 | 0.21 | 29.17 |
| **$Ni/ZrO_2$-800** | 14.13 | 0.14 | 44.41 |

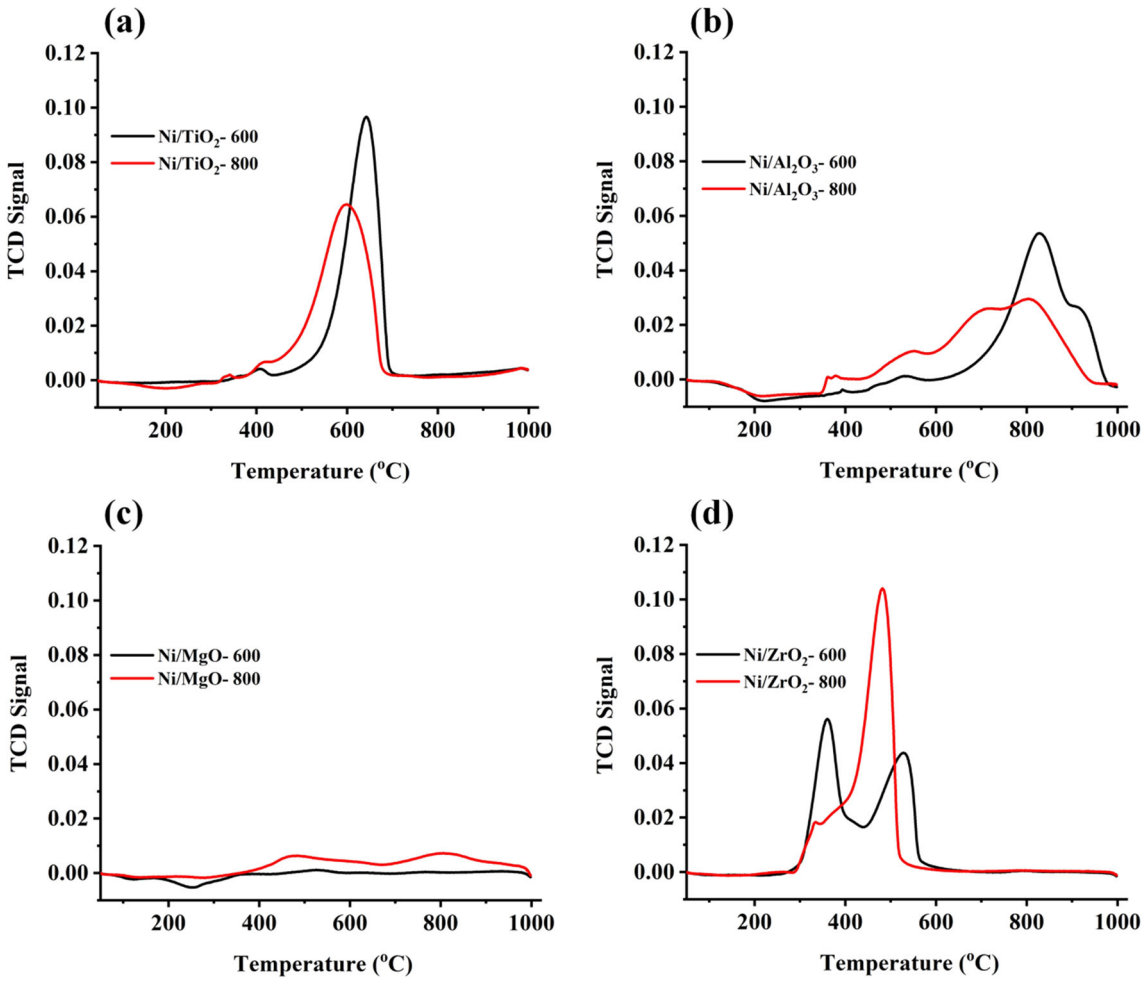


**Fig. 3** $H_2$-temperature programmed reduction profile of catalysts (**a**) Ni/$TiO_2$-600 and Ni/$TiO_2$-800 (**b**) Ni/$Al_2O_3$-600 and Ni/$Al_2O_3$-800 (**c**) Ni/MgO-600 and Ni/MgO-800 (**d**) Ni/$ZrO_2$-600 and Ni/$ZrO_2$-800

and the strengthening of bond strength between NiO and another metal M′ (NiO–M′ bond). The infrared peak beyond 1000 $cm^{-1}$ is due to "$CO_2$-interacting surface species" and surface hydroxyl.

The Titania-supported Ni catalyst has a band related chiefly to stretching and bending vibration of OH at 3425 $cm^{-1}$ and 1625 $cm^{-1}$ respectively (Fig. 4a). Interestingly, if a titania-supported Ni catalyst is prepared at a higher calcination temperature (800 °C), the band of these hydroxyl groups is intensified (Fig. 4b, c) and the intensity of these bonds at Ni/$TiO_2$-800 is greater than that of other catalysts. $TiO_2$-supported Ni catalysts have a peak between 400 and 800 $cm^{-1}$ corresponding to Ti–O bending and stretching vibrations [37]. The vibrational peak due to Ni–O is not specified over the given IR spectra, or it may merge with the broad vibration peak of Ti–O (Fig. 4c). It is observed that at a higher calcination temperature (800 °C), the intensity of the vibration band of Ti–O decreases indicating a possible interaction of Ti–O with another metal at a higher calcination temperature.

If the $ZrO_2$-supported Ni catalyst is synthesized at a high calcination temperature (800 °C), the intensity of the hydroxyl band is decreased compared to the catalyst calcined at a lower calcination temperature (600 °C) (Fig. 4f). This observation is just the reverse of the $TiO_2$-supported Ni catalyst. Zirconia-supported Ni catalyst calcined at lower temperatures has a peak at 422 $cm^{-1}$, which indicates the strengthening of the bond between NiO and support metal (NiO-M′ bond). Simply, it indicates the increased metal-support interaction (then an IR vibration peak at 433 $cm^{-1}$ for free NiO). Apart from these, there are also several vibration peaks at 496 $cm^{-1}$, 550 $cm^{-1}$, 584 $cm^{-1}$, 629 $cm^{-1}$, and 750 $cm^{-1}$ for Zr-O bond vibration [15, 38].

IR spectra MgO-supported Ni catalysts have peculiarities in means of the band for surface $CO_2$-species. It has a diffuse peak at 859 $cm^{-1}$ for ionic $CO_3^{2-}$ [37–39], a broadband (consisting of several overlapping peaks from 1460 $cm^{-1}$,

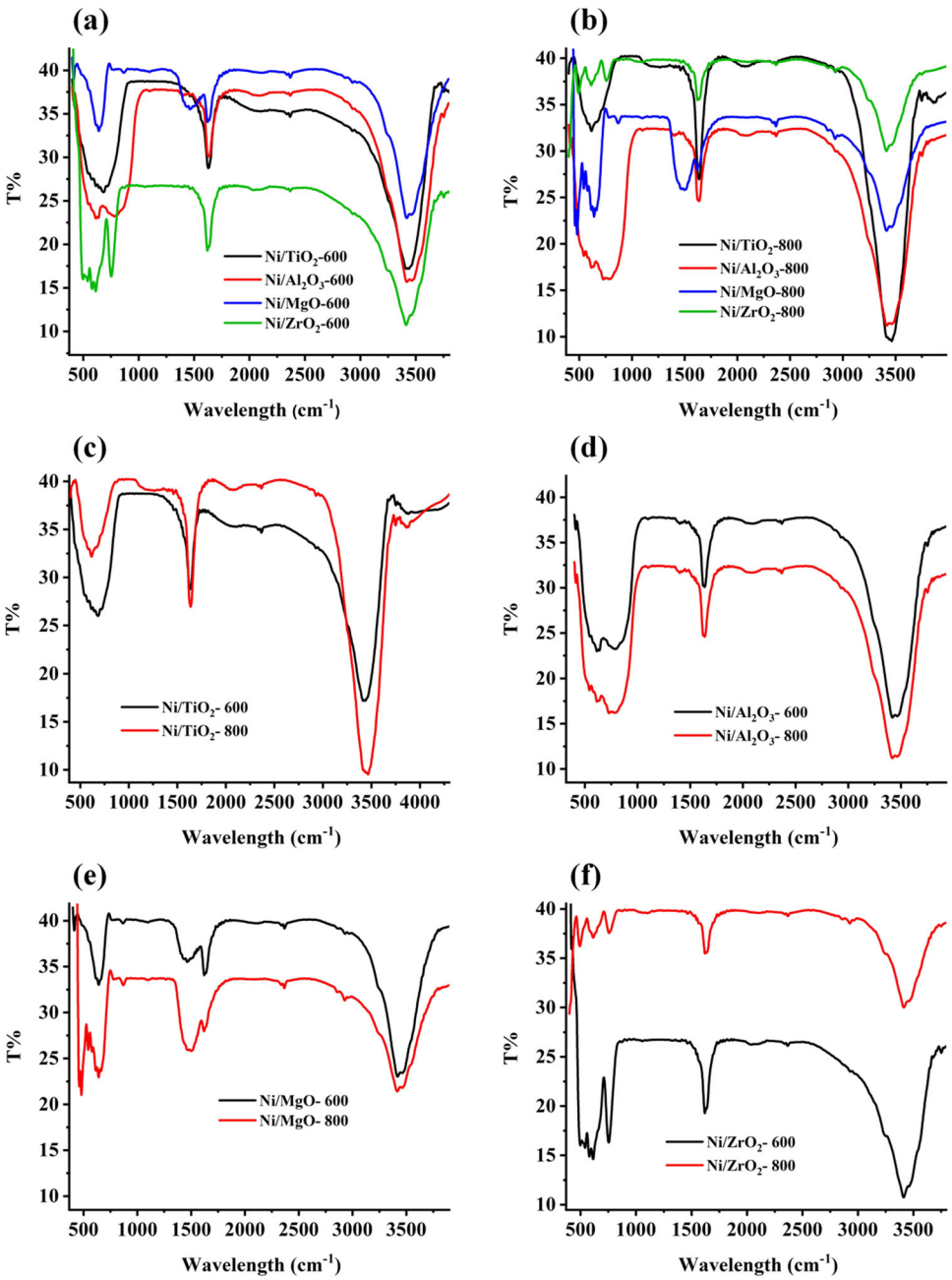


**Fig. 4** Infrared transmittance spectra of (**a**) all catalysts calcined at 600 °C (**b**) all catalysts calcined at 800 °C (**c**) $Ni/TiO_2$-600 and $Ni/TiO_2$-800 (**d**) $Ni/Al_2O_3$-600 and $Ni/Al_2O_3$-800 (**e**) Ni/MgO-600 and Ni/MgO-800 (**f**) $Ni/ZrO_2$-600 and $Ni/ZrO_2$-800

1530 $cm^{-1}$ [40] for ionic and unidentate carbonate species (Fig. 4e). It indicates that MgO supported Ni species can absorb $CO_2$ from the environment, interact with it and form various $CO_2$-interacting species on the surface even at room temperature. The effect of calcination temperature on the interaction of $CO_2$ species over the surface is also evident. The peak intensity from 1460 to 1530 $cm^{-1}$ increases if the MgO-supported Ni catalyst is calcined at a high calcination temperature (800 °C). It indicates the potential presence of ionic and unidentate carbonate species over a Ni/MgO-800 catalyst. In the Ni/MgO-600 catalyst, the Ni–O vibration peak is observed at 425 $cm^{-1}$ whereas, over the Ni/MgO-800 catalyst, this peak is shifted to 461 $cm^{-1}$. It indicates that if MgO-supported catalysts are prepared at higher calcination temperatures, the NiO interaction with the support is weakened. Another peak at 660 $cm^{-1}$ is due to the stretching vibration of Mg-O [37].

The infrared vibration peak for alumina-supported Ni is specified in the lower temperature peaks at 407 $cm^{-1}$ and a broad peak from 500 to 1000 $cm^{-1}$ (Fig. 4d). The peak at 407 $cm^{-1}$ is attributed to the vibration peak of strongly interacted NiO species with support (NiO-M′). The broad

peak includes the vibration peak of Al-O in $AlO_6$ octahedral units as well as $AlO_4$ tetrahedral units [36, 41].

$CH_4$-temperature programmed surface reaction (TPSR) experiment is carried out up to temperature 875 °C for the different catalyst systems (Fig. 5a, b). The $CH_4$-TPSR peaks at different temperature signify the extent of $CH_4$ decomposition over different active sites at the catalyst. The peaks of about 600 °C and > 800 °C were claimed to be the decomposition of $CH_4$ at Ni-M interface and thermally derived decomposition of $CH_4$ respectively [42]. Catalysts calcined at lower calcination temperature show a prominent $CH_4$ decomposition peak at about 600 °C temperature, which is attributed to $CH_4$ decomposition at the Ni-M (M = Al, Zr, Mg, Ti) interface. The peak intensity of Ni/$ZrO_2$-600 is maximum, and Ni/MgO-600 is minimum. Interestingly, when catalysts are prepared at high calcination temperatures, a distinct surface characteristic for $CH_4$ decomposition is noticed. The $CH_4$ decomposition peak over Ni/$ZrO_2$-800 is not affected (than Ni/$ZrO_2$-600), whereas this peak is markedly suppressed over Ni/$TiO_2$-800 and Ni/MgO-800. Ni/$Al_2O_3$-800 shows multiple $CH_4$ decomposition sites at 550 °C, 700 °C and 800 °C. We have also checked the $CO_2$ interaction profile of Ni/$Al_2O_3$ and Ni/$ZrO_2$ catalyst (calcined at 600 °C and 800 °C) through $CO_2$-temperature programmed desorption experiments (Fig. 5c, d). The $CO_2$ desorption peaks at about 75 °C, 200–400 °C and 750 °C are assigned for weak basic sites, intermediate strength basic sites and strong basic sites, respectively [43]. It is observed that Ni/$Al_2O_3$ catalysts (either calcined at 600 °C or 800 °C) have rich moderate strength basic sites, but Ni/$ZrO_2$-600 has a diffuse population of moderate strength basic sites. Ni/$ZrO_2$ catalyst calcined at high temperature has gained a high population of strong basic sites, about 800 °C. However, these basic sites do not remain useful for catalytic purpose because the DRM reaction is carried out at 700 °C.

DRM is considered as a two-step reaction namely, dissociation of $CH_4$ into $CH_{4-x}$ (x = 1–4) overactive sites and sequential oxidation of $CH_{4-x}$ (x = 1–4) by $CO_2$. In this run, polymerization of $CH_{4-x}$ (x = 1–4) surface-intermediate cannock be neglected which lodges the catalyst with coke [44]. The shading of catalytic active sites by inert coke may harm the catalytic activity seriously. Quantitative/qualitative study of coke deposits over the catalyst surface is needed. The thermogravimetry profile of the spent catalyst system is shown in Fig. 6a. In the course of coke deposition, the MgO-supported Ni catalyst as well as the $Al_2O_3$-supported Ni catalyst was not affected by calcination temperature. The earlier one shows coke resistance, whereas the later one shows extreme coke lodging. Spent Ni/MgO-600 and Spent Ni/MgO-800 show 12–13% weight loss, whereas Spent Ni/$Al_2O_3$-600 and Spent Ni/$Al_2O_3$-800 show 80–82% weight loss. The coke resistance capacity of titania-supported Ni catalyst and zirconia-supported Ni catalyst improved if these catalysts were synthesized at high-calcination temperatures (800 °C). Ni/$TiO_2$-600 and Ni/$TiO_2$-800 catalysts show ~ 60% and 43.4% weight loss, respectively, whereas Ni/$ZrO_2$-600 and Ni/$ZrO_2$-800 catalysts have ~ 79% and ~ 63% weight loss, respectively.

To shed more light on the type of carbon deposit, a Raman spectroscopy study of catalyst samples is carried out (Fig. 6b–e). The spent catalyst system showed a C-O symmetric stretching vibration peak of ionic carbonate ($CO_3^{2-}$ group) at 1055 $cm^{-1}$ [45–47] defects carbon band ($I_D$) at 1340 $cm^{-1}$, graphite carbon band ($I_G$) about 1573 $cm^{-1}$ and the 2D band about 2680 $cm^{-1}$. The defect band is due to vibrations of carbon atoms with dangling bonds in an amorphous carbon network, whereas graphite carbon corresponds to the stretching vibration of highly symmetric carbon $sp^2$ bonds [48]. The spent $TiO_2$-supported Ni catalyst and spent $Al_2O_3$-supported Ni catalyst which are calcined at a high temperature (800 °C) have a higher intensity of defect carbon bands ($I_D$) and 2D carbon bands than the catalyst calcined at a low temperature (Fig. 6b, c). In the case of zirconia-supported Ni catalyst, the opposite is true. That means, higher temperature calcined spent Ni/$ZrO_2$-800 catalyst has low-intensity carbon bands (Fig. 6e). For the spent Ni/MgO-800 catalyst, the peak for carbonate has maximum intensity (Fig. 6d). Among all, spent Ni/$Al_2O_3$-800 has the highest intensity of all types of carbon bands, including a band of about 2185 $cm^{-1}$ for the presence of C≡C [49].

### 3.2 Catalyst Activity Result

The catalytic activity in terms of $H_2$-yield of different catalyst systems toward the DRM reaction is shown in Fig. 7a, b. The activity of pure NiO is also tested for dry reforming of methane. The $H_2$-yield and CO-yield is just 0.75% and 1.25% respectively at 700 °C reaction temperature over pure NiO (not shown in Fig. 7). Clearly, the size and stability of Ni against high temperature in DRM are a crucial factor in achieving high activity. In search of Ni stability, the catalyst prepared by dispersion of 5wt% Ni over thermally sustainable metal oxide supports like titania, magnesium oxide, alumina, and zirconia are tested for DRM reaction. Titania-supported Ni catalyst calcined at 600 °C is crystalline (having both rutile and anatase $TiO_2$ phases). It has low surface area, prominent presence of surface hydroxyl (-OH) and reducible "moderately interacted NiO-species". Espinbs et al. showed the diffusion of metallic Ni into $TiO_x$ layer > 500 °C temperature [50]. They showed growth of NiO island due to the presence of $TiO_2$. E. Ruckenstein et al. showed migration of $Ni^{+2}$ ion into the $TiO_2$ layer [51]. Simoens et al. showed the migration of titanium and oxygen species onto the surface of Ni during reductive treatment [52]. Here, it can be concluded that migration of metallic Ni from the surface or oxidation of metallic Ni by $TiO_2$ under oxidizing environment (by $CO_2$)

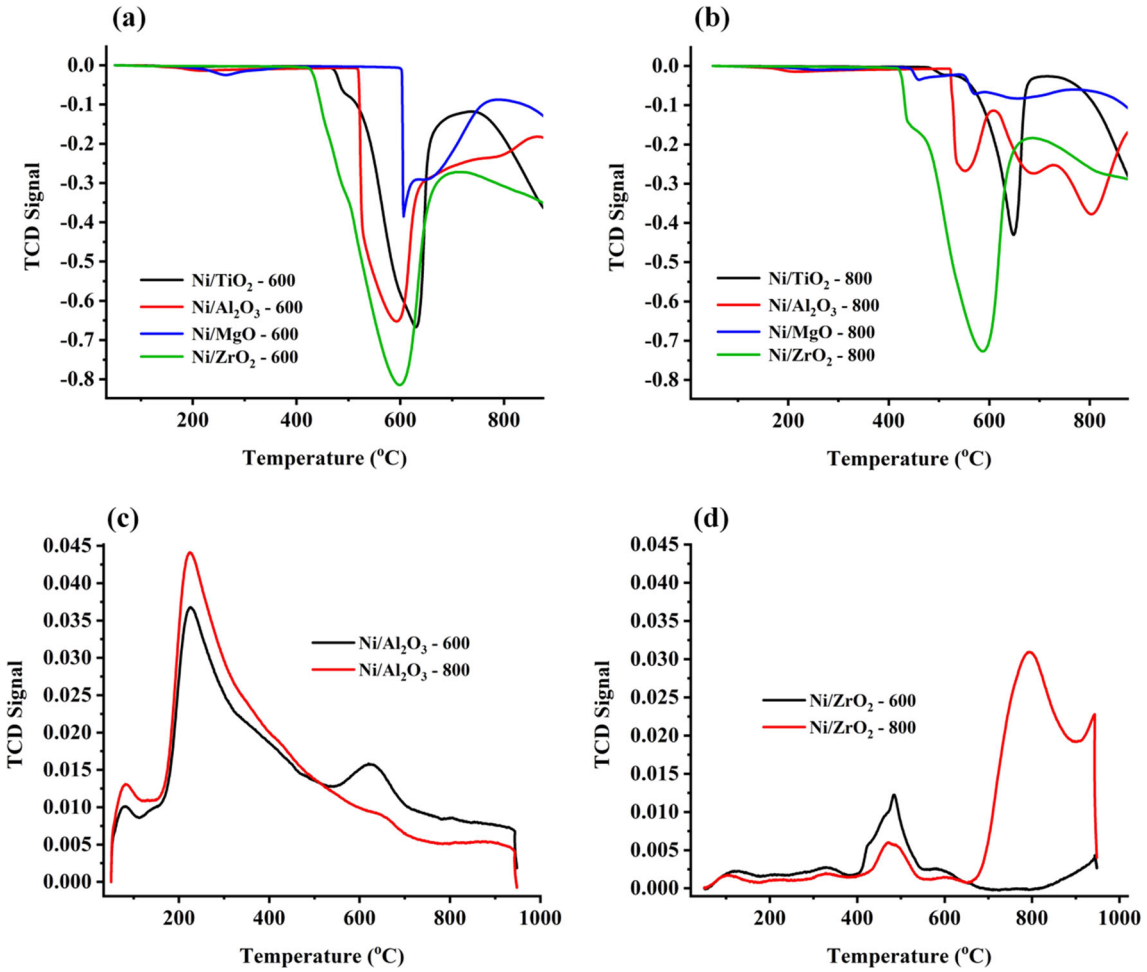


**Fig. 5** $CH_4$-temperature programmed surface reaction profile of (**a**) all catalysts calcined at 600 °C, (**b**) all catalysts calcined at 800 °C, (**c**) $CO_2$-TPD of $Ni/Al_2O_3$-600 and $Ni/Al_2O_3$-800 (**d**) $CO_2$-TPD of $Ni/ZrO_2$-600 and $Ni/ZrO_2$-800

may result in inferior activity toward DRM. $Ni/TiO_2$-600 shows only 35% hydrogen yield, further slowing down to 26% at the 440-min. If the same catalyst is prepared at 800 °C, surface hydroxyl concentration has raised, titania phases are restricted to rutile, additional rhombohedral nickel titanium oxide phase appears, and surface area drops immensely. The intensity of reducible "moderately interacted NiO species" is also got down. $CH_4$-TPSR experiment also shows a marked decrease of $CH_4$ decomposition sites over $Ni/TiO_2$ catalyst if it is prepared at 800 °C calcination temperature. The sharp drop of surface area decreased amount of reducible NiO species and less concentration of $CH_4$ decomposition sites over $Ni/TiO_2$-800, results in more inferior catalytic performance toward DRM. At the end of 440-min, the $H_2$-yield remains at just ~ 22%. The catalyst has an immense carbon deposit during the reaction that may also contribute to the inferiority of the catalyst toward DRM. The CO-yield remains 16% higher (than $H_2$-yield) over $Ni/TiO_2$-600 and 31% higher (than $H_2$-yield) over $Ni/TiO_2$-800 at the end of the reaction (440-min). It indicates the pronounced presence of reverse water gas shift reaction over titania-supported Ni catalyst, which is responsible for consuming $H_2$ and affecting the final $H_2$-yield.

MgO-supported Ni catalyst calcined at 600 °C has a cubic magnesium nickel oxide phase. NiO bonding with support MgO is also verified by IR spectra at wavenumber 425 $cm^{-1}$. But these nickel-containing species seem to be poorly reducible. However, Raman and infrared spectroscopy verify the presence of ionic as well as unidentate carbonate species over the catalyst surface, even under normal environmental conditions. The TGA result also indicates the least carbon deposit over a MgO-supported Ni catalyst. It indicates that the catalyst is quite interactive with $CO_2$ species. The catalytic activity of Ni/MgO-600 is quite impressive. It shows a continuous 54–55% $H_2$ yield up to 430-min. The high $H_2$-yield even the inadequate presence of reducible NiO species indicates that the role of interacting $CO_2$ species is crucial for DRM over MgO-supported Ni catalysts. If the same catalyst is prepared at a high calcination temperature (800 °C), the concentration of $CO_2$-interacting species grows

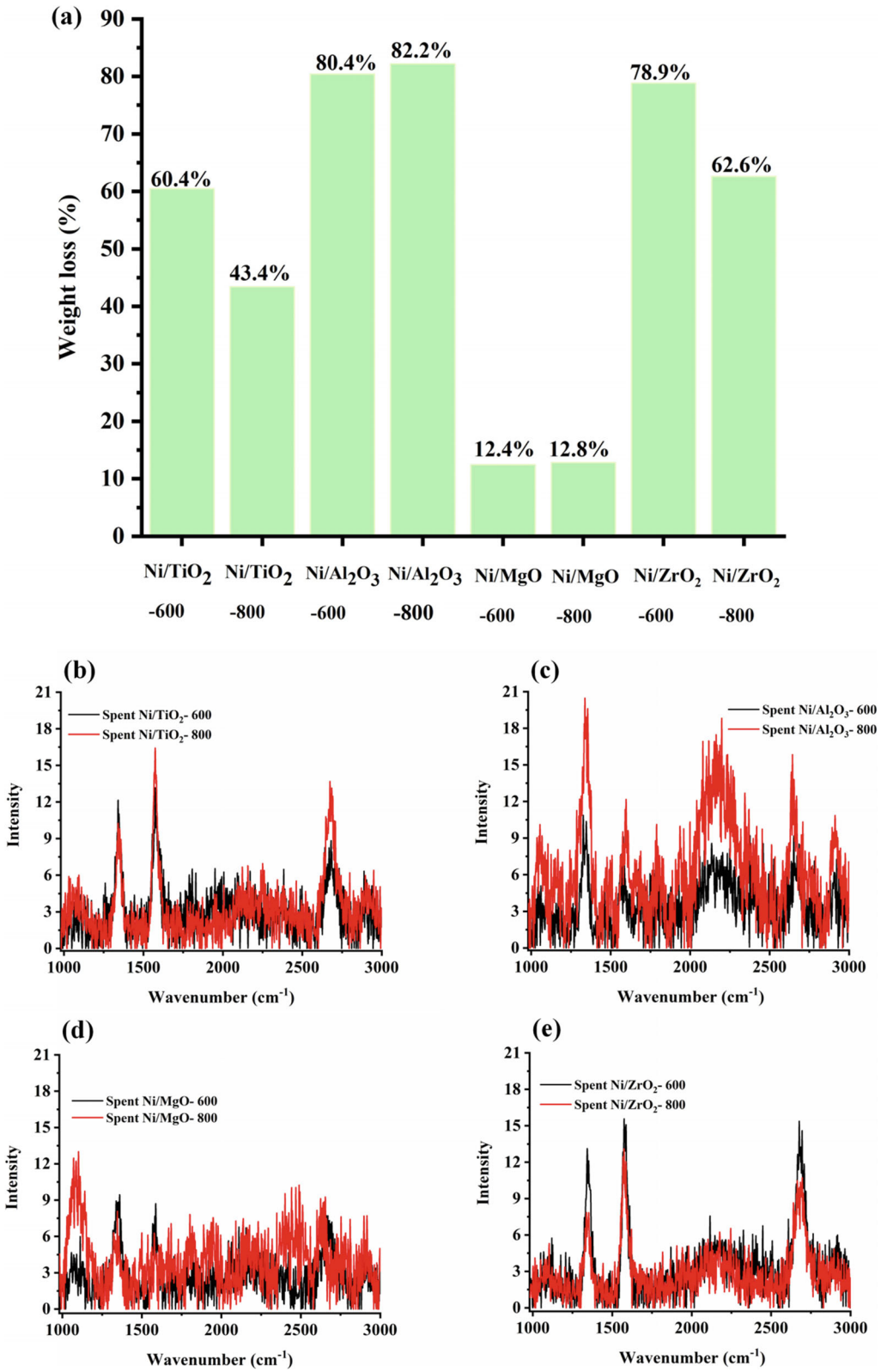


**Fig. 6** (**a**) Thermogravimetry profile of all catalysts calcined at 600 °C and at 800 °C (**b**) Raman spectra of spent $Ni/TiO_2$-600 and spent $Ni/TiO_2$-800 (**c**) Raman spectra of spent $Ni/Al_2O_3$-600 and spent $Ni/Al_2O_3$-800 (**d**) Raman spectra of spent Ni/MgO-600 and spent Ni/MgO-800 (**e**) Raman spectra of spent $Ni/ZrO_2$-600 and spent $Ni/ZrO_2$-800

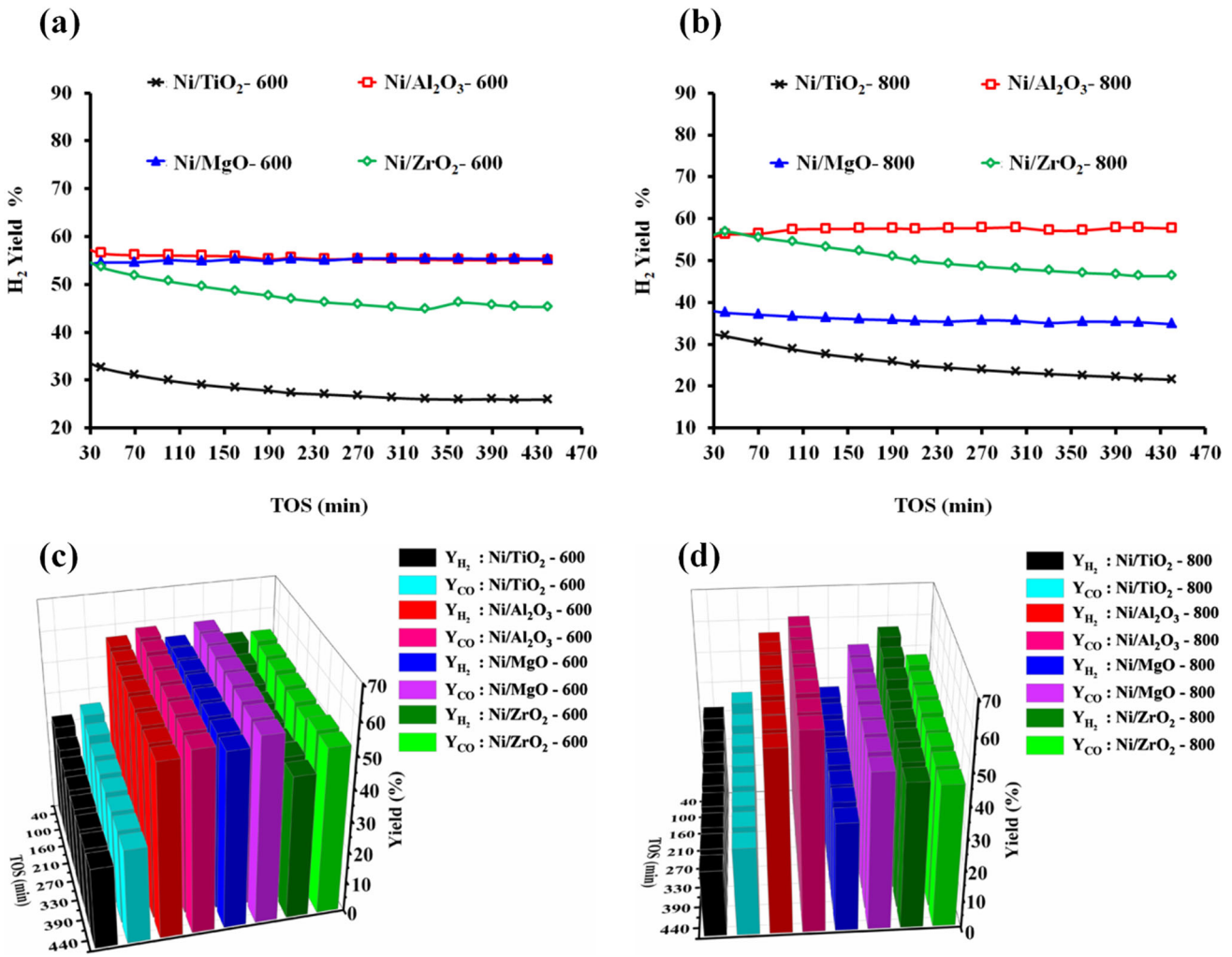


**Fig. 7** Activity results versus TOS (**a**) The $H_2$-Yield vs TOS over Ni/$TiO_2$-600, Ni/$Al_2O_3$-600, Ni/MgO-600, Ni/$ZrO_2$-600 (**b**) The $H_2$-Yield versus TOS over Ni/$TiO_2$-800, Ni/$Al_2O_3$-800, Ni/MgO-800, Ni/$ZrO_2$-800 (**c**) "The $H_2$-Yield and CO-yield" vs TOS over Ni/$TiO_2$-600, Ni/$Al_2O_3$-600, Ni/MgO-600, Ni/$ZrO_2$-600 (**d**) "The $H_2$-Yield and CO-yield" versus TOS over Ni/$TiO_2$-800, Ni/$Al_2O_3$-800, Ni/MgO-800, Ni/$ZrO_2$-800

but the bonding between NiO and support metal is weakened (as observed in IR spectra at 461 $cm^{-1}$). The weak bonding between "NiO and support metal" and substantial decrease in surface area is noticed over Ni/MgO-800. $CH_4$-TPSR experiment shows marked suppression of $CH_4$ decomposition sites over Ni/MgO-800 catalyst. It acquired 38–35% $H_2$-yield during 430-min time on stream. Here, it is also noticeable that the CO-yield remains just 6–8% above than $H_2$-yield during 430-min time on stream over Ni/MgO-600. But over Ni/MgO-800, CO-yield is quite higher (33–44% than $H_2$-yeild) (Fig. 7c, d). That means, weak bonding between "NiO and support metal", suppression of $CH_4$ decomposition sites, and potential consumption of $H_2$ by reverse water gas shift reaction result into inferior catalyst performance than Ni/MgO-800.

Zirconia-supported Ni catalyst calcined at 600 °C shows a strong bond between NiO and support metal (NiO-M′) (as observed in IR spectra at 422 $cm^{-1}$). It has reducible NiO-species which interacts with support through weak and moderate strength. $CH_4$-TPSR experiment shows the highest density of $CH_4$ decomposition sites over Zirconia-supported Ni catalyst. Zirconia-supported Ni catalyst calcined at 800 °C has reducible NiO species which interacts with support through moderate strength. The $CH_4$-TPSR experiment also shows the intensity of $CH_4$ decomposition sites remains equal over Ni/$ZrO_2$ catalyst either it is calcined at 600 °C or 800 °C. Both catalysts Ni/$ZrO_2$-600 and Ni/$ZrO_2$-800 had quite comparable performance. Both show an initial 55–56% $H_2$-yield which drops to 45–46% $H_2$-yield at the end of 430-min. The catalyst either calcined at low temperature (600 °C) or high temperature (800 °C) had very high coke deposits

(79% and 63% respectively). It seems that the strong bond between NiO and support metal (NiO-M′) and the presence of reducible "moderately interacted NiO-species" are the prime cause of initial good catalytic performance. But the activity is seized slowly by heavy coke deposition with time. The performance of $Ni/ZrO_2$-800 is again notable as CO-yield is always found to be less than $H_2$-yield (Fig. 7d). It indicates the inhibition of reverse water gas shift reaction over $Ni/ZrO_2$-800 catalyst.

Alumina-supported Ni catalysts (either calcined at 600 °C or 800 °C) have the highest surface in its series. Relatively, the surface area of the catalyst decreased markedly if it is prepared at a higher calcination temperature (800 °C). Both catalysts have a $NiAl_2O_4$ phase, which exsolves stable metallic Ni upon reduction. The catalyst has the highest coke deposition (80–82%), but both catalysts' activity ($Ni/Al_2O_3$-600 and $Ni/Al_2O_3$-800) is retained at a high (55–58% $H_2$-yield) for up to 430 min. Ni exsolved from $NiAl_2O_4$ seems quite stable, and it restricts the carbon deposit layover at the Ni or Ni–Al boundary. Carbon is deposited away from the active sites and does not affect catalytic activity. The catalyst maintains high $CH_4$ decomposition (into $CH_x$) over stable Ni (exsolved from $NiAl_2O_4$) and transfers the $CH_x$ species away from the catalytic active site. In the meantime, either $CO_2$ (or surface-interacted $CO_2$- species) oxidizes the $CH_x$ species (into $H_2$ and CO) or the $CH_x$ species is left behind for polymerization and subsequent coke formation. The proper matching between the carbon formation rate and carbon diffusion rate (away from the carbon formation site) continually exposes the catalytic site for the fresh reaction [53, 54]. So even against the highest coke deposition, an alumina-supported Ni catalyst maintains 55–58% $H_2$-yield up to 430-min time on stream. The CO-yield was just 1.6–3% higher than the $H_2$-yield over $Ni/Al_2O_3$-600 catalyst and 8–9% higher than the $H_2$-yield over $Ni/Al_2O_3$-800 during 430-min time on steam. It indicates the mark presence of reverse water gas shift reaction also above the alumina-supported Ni catalyst system.

It is time to conclude the reaction mechanism over each catalyst system. $TiO_2$-supported Ni catalyst has active sites Ni, which is derived by the reduction of "moderately interacted NiO species". Masking of active sites Ni by $TiO_2$ results in the least catalytic activity (26% $H_2$-yield) (Fig. 8a). Again, "$Ni/TiO_2$ calcined at a higher temperature" has lower density of $CH_4$ decomposition sites/metallic Ni over diminutive surface area (than the lower temperature calcined catalyst), resulting in the worst $H_2$-yield (22%) at the end of 440-min TOS. MgO-supported Ni catalyst has the least population of active Ni species, but the richest interaction with $CO_2$, resulting in ~ 55% $H_2$-yield with minimum coke deposition (Fig. 8b). If the Ni/MgO catalyst is prepared at a higher calcination temperature, the interaction of active sites with support becomes weaker and catalyst retains minimum density of $CH_4$ decomposition sites. So, Ni/MgO-800 °C turns into inferior activity (35% $H_2$-yield) than Ni/MgO-600. The effect of calcination temperature of $Ni/ZrO_2$ does not affect the population of $CH_4$-decomposition sites. However, the $CO_2$-interaction profile of $Ni/ZrO_2$ catalyst is inferior to $Ni/Al_2O_3$ catalyst. The enhanced metal-support interaction and highest population of $CH_4$ decomposition sites over $Ni/ZrO_2$ offers high DRM activity (~ 55%) initially, which slowed down to 46% $H_2$-yield against high coke deposition (63–79% weight loss) (Fig. 8c). The mark inhibition of RWGS is noticed (CO yield < $H_2$-yield) over zirconia-supported Ni catalyst if it is prepared at high calcination temperature. $Ni/Al_2O_3$ has stable catalytic active metallic Ni sites (exsolved from $NiAl_2O_4$), prominent $CH_4$ decomposition sites and a relatively richer $CO_2$ interaction profile than $Ni/ZrO_2$. The catalytic activity for DRM and coke deposition remains unaffected by calcination temperature over $Al_2O_3$-supported Ni catalyst. Ni exsolved from $NiAl_2O_4$ phase over $Ni/Al_2O_3$ catalyst is quite stable and constantly exposable to feed gas, maintaining high $H_2$-yield (~ 58%) up to 430-min even against the highest coke deposition (Fig. 8d).

The catalytic activity of our catalyst is compared with other "supported NiO-based" system and shown in Table 1. Among dual metal oxide-supported Ni catalyst ($Ni/TiO_x$-$Al_2O_3$, Ni/ $MoO_x$-$Al_2O_3$, $Ni/La_2O_3$-$ZrO_2$, $Ni/CeO_2$-$ZrO_2$, $Ni/Y_2O_3$-$ZrO_2$, Ni/MgO-$ZrO_2$, $Ni/Al_2O_3$-MgO and Ni/CaO- $Al_2O_3$) are prepared by multiple pots synthesis and maximum 44–45% hydrogen yield is achieved over $Ni/Al_2O_3$-MgO and $Ni/Y_2O_3$-$ZrO_2$ [36, 55–59]. Among single metal oxide-supported Ni catalyst, about 45% $H_2$-yield is achieved over Ni/mesoporous $SiO_2$ (prepared with the assistance of oleic acid) and $Ni/ZrO_2$ [55, 59–65]. However, using high-cost carrier gas (helium) for DRM over $Ni/ZrO_2$ may not be encouraged. The current catalyst systems like $Ni/Al_2O_3$ (calcined at 600 °C and 800 °C) are prepared under single pot impregnation methodology. The maximum ~ 58% $H_2$-yield (up to 7 h time on stream at 700 °C reaction temperature) is achieved over $Ni/Al_2O_3$-800.

## 4 Conclusion

Higher calcination temperature during catalyst preparation modifies metal-support interaction, distribution of active species and density of $CH_4$ decomposition sites and substantial collapse of smaller pores into larger one (resulting in smaller surface area). At higher calcination temperature (800 °C), $CH_4$ decomposition sites over "titania-supported Ni catalyst" and "magnesia-supported Ni catalyst" are depleted, whereas the surface area of $TiO_2$-supported Ni is dropped abruptly. These cause lower catalytic activity over $Ni/TiO_2$ and Ni/MgO if these catalysts are prepared at 800 °C.

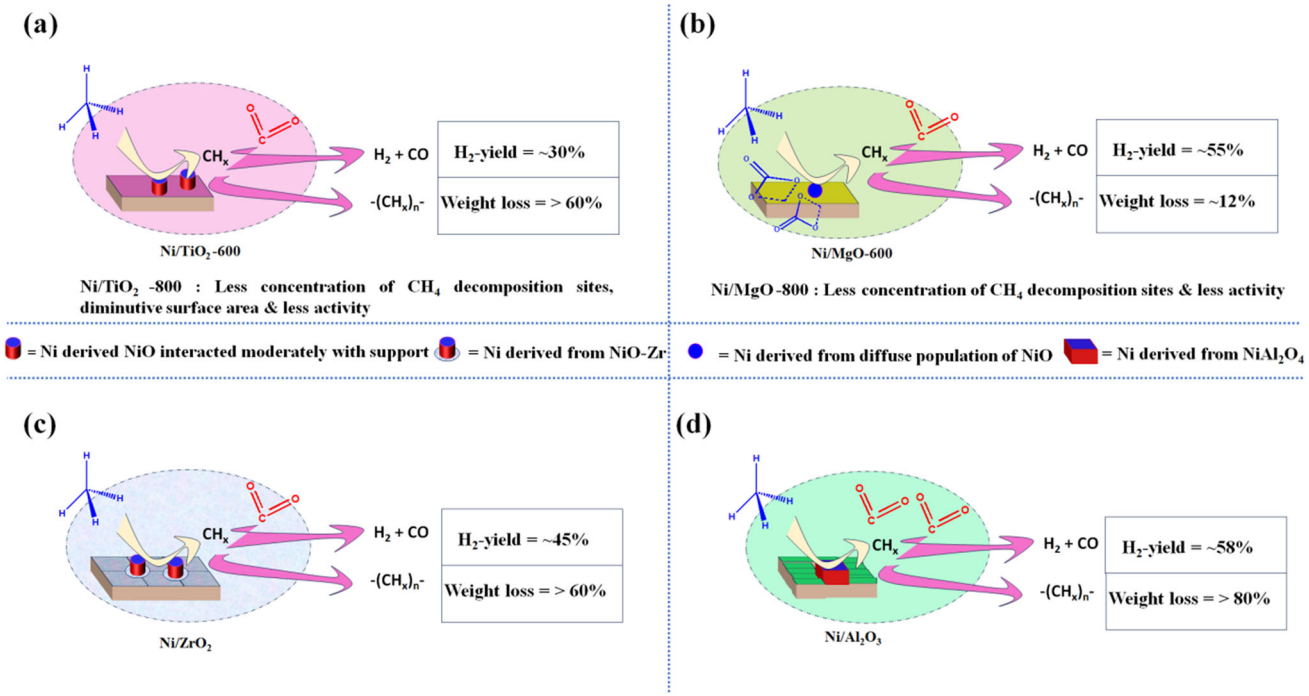


**Fig. 8** Reaction mechanism layout over each catalyst system: (**a**) $CH_4$ decomposition over metallic Ni (derived from moderately interacted NiO species) followed by oxidation by $CO_2$ over Ni/TiO-600 catalyst refereeing least DRM activity and high coke deposition (**b**) $CH_4$ decomposition over available Ni sites followed by oxidation by $CO_2$ and $CO_2$-interacting species over Ni/MgO-600 catalyst resulting high DRM activity and least coke deposition (**c**) $CH_4$ decomposition over metallic Ni derived from strongly interacted NiO-Zr species followed by oxidation by $CO_2$ causing high DRM activity against high coke deposition (**d**) $CH_4$ decomposition over metallic Ni exsolved from $NiAl_2O_4$ followed by oxidation by $CO_2$ causing highest DRM activity against highest coke deposition

**Table 1** Comparative table of catalytic activity ($H_2$-yieid) over different catalyst systems

| Sl. no | Active Metal | Support | Feed ratio $CH_4$:$CO_2$: Carrier gas ($N_2$) | Preparation method, reaction time, reaction temperature, WHSV | $H_2$ Yield (%) | References |
|---|---|---|---|---|---|---|
| 1 | Ni | $Al_2O_3$ | 1: 1: 0 | Ultra-sonication assisted impregnation, 70 h, 600 °C, 70L/$hg_{cat}$ | 22 | [60] |
| 2 | Ni | $Al_2O_3$ | 1: 1: 3 | Impregnation, 5 h, 550 °C, 60L/$hg_{cat}$ | 12 | [61] |
| 3 | Ni | $Al_2O_3$ | 1: 1: 0 | Impregnation, 24 h, 550 °C, 24L/$hg_{cat}$ | 10 | [62] |
| 4 | Ni | $Al_2O_3$ | 1: 1: 0 | Impregnation, 24 h, 650 °C, 24L/$hg_{cat}$ | 30 | [62] |
| 5 | Ni | $Al_2O_3$ | 3: 2: 50 (He) | Impregnation, 850 °C, 120L/$hg_{cat}$ | 39 | [59] |
| 6 | Ni | $ZrO_2$ | 3: 3: 1 | Impregnation, 7 h, 700 °C, 42L/$hg_{cat}$ | 43 | [63] |
| 7 | Ni | $ZrO_2$ | 55: 35: 10 | Impregnation, 10 h, 800 °C, 40L/$hg_{cat}$ | 10 | [55] |
| 8 | Ni | $ZrO_2$ | 1: 1: 2 (Ar) | Impregnation, 0.5 h, 700 °C, 60L/$hg_{cat}$ | 45 | [64] |
| 9 | Ni | $TiO_x$-$Al_2O_3$ | 3: 3: 1 | Impregnation, 7 h, 700 °C, 12L/$hg_{cat}$ | 30 | [36] |

**Table 1** (continued)

| Sl. no | Active Metal | Support | Feed ratio $CH_4$:$CO_2$: Carrier gas ($N_2$) | Preparation method, reaction time, reaction temperature, WHSV | $H_2$ Yield (%) | References |
|---|---|---|---|---|---|---|
| 10 | Ni | $MoO_x$-$Al_2O_3$ | 3: 3: 1 | Impregnation, 7 h, 700 °C, 12L/$hg_{cat}$ | 39 | [36] |
| 11 | Ni | $La_2O_3$-$ZrO_2$ | 55: 35: 10 | Impregnation, 10 h, 800 °C, 120L/$hg_{cat}$ | 11 | [55] |
| 12 | Ni | $CeO_2$-$ZrO_2$ | 55: 35: 10 | Impregnation, 10 h, 800 °C, 120L/$hg_{cat}$ | 13 | [55] |
| 13 | Ni | $Y_2O_3$-$ZrO_2$ | 3: 3: 1 | Sol–Gel, 7 h, 700 °C, 42L/$hg_{cat}$ | 45 | [56] |
| 14 | Ni | MgO-$ZrO_2$ | 3: 3: 1 | Sol–Gel, 7 h, 700 °C, 42L/$hg_{cat}$ | 23 | [56] |
| 15 | Ni | Mesoporous $SiO_2$ | 1: 1: 0 | Oleic acid assisted impregnation, 6 h, 700 °C, 24L/$hg_{cat}$ | 45 | [65] |
| 16 | Ni | Mesoporous $SiO_2$ | 1: 1: 0 | Impregnation, 6 h, 700 °C, 24L/$hg_{cat}$ | 32 | [65] |
| 17 | Ni | $Al_2O_3$-MgO | 1: 1: 0 | Sol–Gel, 10 h,650 °C, 24L/$hg_{cat}$ | 44 | [57] |
| 18 | Ni | $CeO_2$-$ZrO_2$ | 1: 1: 0 | Co-precipitation than – Impregnation, 24 h, 700 °C, 30L/$hg_{cat}$ | 34 | [58] |
| 19 | Ni | CaO- $Al_2O_3$ | 3: 2: 50 (He) | Impregnation, 850 °C, 120L/$hg_{cat}$ | 40 | [59] |
| 20 | Ni | MgO- $Al_2O_3$ | 3: 2: 50 (He) | Impregnation, 850 °C, 120L/$hg_{cat}$ | 36 | [59] |
| 21 | Ni | $Al_2O_3$-600 | 3: 3: 1 | Impregnation, 7 h, 700 °C, 42L/$hg_{cat}$ | 55.05 | This study |
| 22 | Ni | $Al_2O_3$-800 | 3: 3: 1 | Impregnation, 7 h, 700 °C, 42L/$hg_{cat}$ | 57.65 | |

The density of $CH_4$-decomposition sites remains unaffected over Ni/$ZrO_2$, whereas the surface area of Ni/$Al_2O_3$ remains highest in its series even upon higher calcination temperature. Titania-supported Ni catalyst is found to be inferior toward DRM. The MgO-supported Ni catalyst, calcined at 600 °C, has excellent interaction with $CO_2$, the least carbon deposit, strong bond between NiO-support but inadequate presence of reducible NiO species. It showed quite a high $H_2$-yield (~ 55%) up to 430-min on stream. The strong bond between NiO and support metal (NiO-Zr), the population of reducible "moderately interacted NiO species" and the highest population of $CH_4$ decomposition sites over zirconia-supported Ni catalyst results in a high $H_2$ yield of ~ 55%. However, it slowed down to ~ 45% during the 430-min on stream due to heavy coke deposition. The potential inhibition of reverse water gas shift reaction over Ni/$ZrO_2$-800 makes it unique to rest catalyst systems. Alumina-supported Ni catalysts have a $NiAl_2O_4$ phase and high surface area. Ni exsolved from $NiAl_2O_4$ at 700 °C during catalyst activation is relatively stable and active. It catalyzes $CH_4$ decomposition (into $CH_x$) at stable Ni and transfers the fragment $CH_x$ away from the active sites where further oxidation (by $CO_2$) or polymerization of $CH_x$ species occurs. It resulted in a constant high 55–58% $H_2$-yield even against high coke deposition during the 430-min on stream.

**Supplementary Information** The online version contains supplementary material available at https://doi.org/10.1007/s13369-023-08576-0.

**Acknowledgements** The authors extend their appreciation to the Deputyship for Research and Innovation, "Ministry of Education" in Saudi Arabia for funding this research (IFKSUOR3-426-1). Also, JAD acknowledges Queen's University Belfast for supporting research. RK and NP acknowledge Indus University, Ahmedabad for supporting research.

## References


1. Mazloomi, K.; Gomes, C.: Hydrogen as an energy carrier: Prospects and challenges. Renew. Sustain. Energy Rev. **16**, 3024–3033 (2012). https://doi.org/10.1016/j.rser.2012.02.028
2. Mashayekhi, F.: The effects of molar ratio and calcination temperature on NiO nanoparticles' properties. Int. Nano Lett. **12**, 273–279 (2022). https://doi.org/10.1007/s40089-022-00371-3
3. Silva, V.D.; Nascimento, E.P.; Grilo, J.P.F.; Simões, T.A.; Menezes, R.R.; Macedo, D.A.; Medeiros, E.S.: Effect of two-step calcination on the formation of nickel oxide hollow nanofibers. Open Ceram. **5**, 100087 (2021). https://doi.org/10.1016/j.oceram.2021.100087
4. Shand, M.A.: The Chemistry and Technology of Magnesia. (2006). https://books.google.co.in/books?id=7L5TAAAAMAAJ
5. Jafarbegloo, M.; Tarlani, A.; Mesbah, A.W.; Muzart, J.; Sahebdelfar, S.: NiO-MgO solid solution prepared by sol–gel method as precursor for Ni/MgO Methane Dry reforming catalyst: effect of calcination temperature on catalytic performance. Catal. Letters. **146**, 238–248 (2016). https://doi.org/10.1007/s10562-015-1638-9
6. Usman, M.; Wan Daud, W.M.A.: An investigation on the influence of catalyst composition, calcination and reduction temperatures on Ni/MgO catalyst for dry reforming of methane. RSC Adv. **6**, 91603–91616 (2016). https://doi.org/10.1039/c6ra15256b
7. Shah, M.; Al Mesfer, M.K.; Danish, M.: Effect of titania synthesis conditions on the catalytic performance of mesoporous Ni/$TiO_2$ catalysts for carbon dioxide reforming of methane. Int. J. Hydrog. Energy **47**, 8867–8874 (2022). https://doi.org/10.1016/j.ijhydene.2021.12.246
8. Zhang, Z.-Y.; Zhang, T.; Liang, W.-P.; Bai, P.-W.; Zheng, H.-Y.; Lei, Y.; Hu, Z.; Xie, T.: Promoted solar-driven dry reforming of methane with Pt/mesoporous-$TiO_2$ photo-thermal synergistic catalyst: performance and mechanism study. Energy Convers. Manag. **258**, 115496 (2022). https://doi.org/10.1016/j.enconman.2022.115496
9. Shah, M.; Bordoloi, A.; Nayak, A.K.; Mondal, P.: Effect of Ti/Al ratio on the performance of Ni/$TiO_2$-$Al_2O_3$ catalyst for methane reforming with $CO_2$. Fuel Process. Technol. **192**, 21–35 (2019). https://doi.org/10.1016/j.fuproc.2019.04.010
10. Zhang, X.; Wang, F.; Song, Z.; Zhang, S.: Comparison of carbon deposition features between Ni/$ZrO_2$ and Ni/SBA-15 for the dry reforming of methane. React. Kinet. Mech. Catal. **129**, 457–470 (2020). https://doi.org/10.1007/s11144-019-01707-5
11. Khatri, J.; Fakeeha, A.H.; Kasim, S.O.; Lanre, M.S.; Abasaeed, A.E.; Ibrahim, A.A.; Kumar, R.; Al-Fatesh, A.S.: Ceria promoted phosphate-zirconia supported Ni catalyst for hydrogen rich syngas production through dry reforming of methane. Int. J. Energy Res. **45**, 19289–19302 (2021). https://doi.org/10.1002/er.7026
12. Xu, B.Q.; Wei, J.M.; Yu, Y.T.; Li, J.L.; Zhu, Q.M.: Carbon dioxide reforming of methane over nanocomposite Ni/$ZrO_2$ catalysts. Top. Catal. **22**, 77 (2003). https://doi.org/10.1023/A:1021419929938
13. Wang, Y.; Zhao, Q.; Wang, Y.; Hu, C.; Da Costa, P.: One-step synthesis of highly active and stable Ni-$ZrO_x$ for dry reforming of methane. Ind. Eng. Chem. Res. **59**, 11441–11452 (2020). https://doi.org/10.1021/acs.iecr.0c01416
14. Lou, Y.; Steib, M.; Zhang, Q.; Tiefenbacher, K.; Horváth, A.; Jentys, A.; Liu, Y.; Lercher, J.A.: Design of stable Ni/$ZrO_2$ catalysts for dry reforming of methane. J. Catal. **356**, 147–156 (2017). https://doi.org/10.1016/j.jcat.2017.10.009
15. Patel, R.; Fakeeha, A.H.; Kasim, S.O.; Sofiu, M.L.; Ibrahim, A.A.; Abasaeed, A.E.; Kumar, R.; Al-Fatesh, A.S.: Optimizing yttria-zirconia proportions in Ni supported catalyst system for $H_2$ production through dry reforming of methane. Mol. Catal. **510**, 111676 (2021). https://doi.org/10.1016/j.mcat.2021.111676
16. Thommes, M.; Kaneko, K.; Neimark, A.V.; Olivier, J.P.; Rodriguez-Reinoso, F.; Rouquerol, J.; Sing, K.S.W.: Physisorption of gases, with special reference to the evaluation of surface area and pore size distribution (IUPAC Technical Report). Pure Appl. Chem. **87**, 1051–1069 (2015). https://doi.org/10.1515/pac-2014-1117
17. Abasaeed, A.E.; Lanre, M.S.; Kasim, S.O.; Ibrahim, A.A.; Osman, A.I.; Fakeeha, A.H.; Alkhalifa, A.; Arasheed, R.; Albaqi, F.; Kumar, N.S.; Khan, W.U.; Kumar, R.; Frusteri, F.; Al-Fatesh, A.S.; Bagabas, A.A.: Syngas production from methane dry reforming via optimization of tungsten trioxide-promoted mesoporous γ-alumina supported nickel catalyst. Int. J. Hydrog. Energy **48**, 26492–26505 (2022). https://doi.org/10.1016/j.ijhydene.2022.09.313
18. Al-Fatesh, A.S.; Golaviya, J.; Shrivastava, V.K.; Ibrahim, A.A.; Osman, A.I.; Fakeeha, A.H.; Abasaeed, A.E.; Bagabas, A.A.; Lanre, M.S.; Kumar, R.; Hussain, A.; Lin, K.-S.: A highly active and cost-effective tungsten modified Ni-based catalyst for the production of hydrogen via methane dry reforming. Catal. Commun. **171**, 106510 (2022). https://doi.org/10.1016/j.catcom.2022.106510
19. Al-Fatesh, A.S.A.; Fakeeha, A.H.: Effects of calcination and activation temperature on dry reforming catalysts. J. Saudi Chem. Soc. **16**, 55–61 (2012). https://doi.org/10.1016/j.jscs.2010.10.020
20. Bian, Z.; Zhong, W.; Yu, Y.; Wang, Z.; Jiang, B.; Kawi, S.: Dry reforming of methane on Ni/mesoporous-$Al_2O_3$ catalysts: Effect of calcination temperature. Int. J. Hydrog. Energy **46**, 31041–31053 (2021). https://doi.org/10.1016/j.ijhydene.2020.12.064
21. He, L.; Ren, Y.; Yue, B.; Tsang, S.C.E.; He, H.: Tuning metal—support interactions on ni/$Al_2O_3$ catalysts to improve catalytic activity and stability for dry reforming of methane. Processes. **9**, 706 (2021). https://doi.org/10.3390/pr9040706
22. Qiu, H.; Ran, J.; Huang, X.; Ou, Z.; Niu, J.: Unrevealing the influence that preparation and reaction parameters have on Ni/$Al_2O_3$ catalysts for dry reforming of methane. Int. J. Hydrog. Energy **47**, 34066–34074 (2022). https://doi.org/10.1016/j.ijhydene.2022.08.014
23. Medeiros, R.L.B.A.; Figueredo, G.P.; Macedo, H.P.; Oliveira, A.S.; Rabelo-Neto, R.C.; Melo, D.M.A.; Braga, R.M.; Melo, M.A.F.: One-pot microwave-assisted combustion synthesis of Ni-$Al_2O_3$ nanocatalysts for hydrogen production via dry reforming of methane. Fuel (2021). https://doi.org/10.1016/j.fuel.2020.119511
24. Zhang, Q.; Wang, J.; Ning, P.; Zhang, T.; Wang, M.; Long, K.; Huang, J.: Dry reforming of methane over Ni/SBA-15 catalysts prepared by homogeneous precipitation method. Korean J. Chem. Eng. **34**, 2823–2831 (2017). https://doi.org/10.1007/s11814-017-0182-2
25. Song, Y.Q.; Liu, H.M.; He, D.H.: Effects of hydrothermal conditions of $ZrO_2$ on catalyst properties and catalytic performances of Ni/$ZrO_2$ in the partial oxidation of methane. Energy Fuels **24**, 2817–2824 (2010). https://doi.org/10.1021/ef1000024
26. Chen, C.A.; Huang, Y.S.; Chung, W.H.; Tsai, D.S.; Tiong, K.K.: Raman spectroscopy study of the phase transformation on nanocrystalline titania films prepared via metal organic vapour deposition. J. Mater. Sci. Mater. Electron. **20**, 303–306 (2009). https://doi.org/10.1007/S10854-008-9595-3
27. Zhang, W.F.; He, Y.L.; Zhang, M.S.; Yin, Z.; Chen, Q.: Raman scattering study on anatase $TiO_2$ nanocrystals. J. Phys. D Appl. Phys. **33**, 912–916 (2000). https://doi.org/10.1088/0022-3727/33/8/305
28. Li, C.; Li, M.: UV Raman spectroscopic study on the phase transformation of $ZrO_2$, $Y_2O_3$-$ZrO_2$ and $SO_4^{2-}$/$ZrO_2$. J. Raman Spectrosc. **33**, 301–308 (2002). https://doi.org/10.1002/jrs.863
29. Al-Fatesh, A.S.; Patel, R.; Srivastava, V.K.; Ibrahim, A.A.; Naeem, M.A.; Fakeeha, A.H.; Abasaeed, A.E.; Alquraini, A.A.; Kumar, R.: Barium-promoted Yttria–zirconia-supported Ni catalyst for hydrogen production via the dry reforming of methane: role of barium in

the phase stabilization of cubic $ZrO_2$. ACS Omega **7**, 16468–16483 (2022). https://doi.org/10.1021/acsomega.2c00471
30. Basahel, S.N.; Ali, T.T.; Mokhtar, M.; Narasimharao, K.: Influence of crystal structure of nanosized $ZrO_2$ on photocatalytic degradation of methyl orange. Nanoscale Res. Lett. **10**, 73 (2015). https://doi.org/10.1186/s11671-015-0780-z
31. Li, Y.; Sun, X.; Li, H.; Wang, S.; Wei, Y.: Preparation of anatase $TiO_2$ nanoparticles with high thermal stability and specific surface area by alcohothermal method. Powder Technol. **194**, 149–152 (2009). https://doi.org/10.1016/j.powtec.2009.03.041
32. Tian, G.; Fu, H.; Jing, L.; Tian, C.: Synthesis and photocatalytic activity of stable nanocrystalline $TiO_2$ with high crystallinity and large surface area. J. Hazard. Mater. **161**, 1122–1130 (2009). https://doi.org/10.1016/j.jhazmat.2008.04.065
33. Zhang, C.; Hu, X.; Zhang, Z.; Zhang, L.; Dong, D.; Gao, G.; Westerhof, R.; Syed-Hassan, S.S.A.: Steam reforming of acetic acid over $Ni/Al_2O_3$ catalyst: correlation of calcination temperature with the interaction of nickel and alumina. Fuel **227**, 307–324 (2018). https://doi.org/10.1016/j.fuel.2018.04.111
34. Fakeeha, A.H.; Patel, R.; El Hassan, N.; Al-Zahrani, S.A.; Al-Awadi, A.S.; Frusteri, L.; Bayahia, H.; Alharth, A.I.; Al-Fatesh, A.S.; Kumar, R.: Holmium promoted yttria-zirconia supported Ni catalyst for $H_2$ production via dry reforming of methane. Int. J. Hydrog. Energy **47**, 38242–38257 (2022). https://doi.org/10.1016/j.ijhydene.2022.09.029
35. Kumar, R.: Surface Characterization Techniques: From Theory to Research. De Gruyter, Berlin, Boston (2022) https://doi.org/10.1515/9783110656480
36. Al-Fatesh, A.S.; Chaudhary, M.L.; Fakeeha, A.H.; Ibrahim, A.A.; Al-Mubaddel, F.; Kasim, S.O.; Albaqmaa, Y.A.; Bagabas, A.A.; Patel, R.; Kumar, R.: Role of mixed oxides in hydrogen production through the dry reforming of methane over nickel catalysts supported on modified $\gamma$-$Al_2O_3$. Processes. **9**, 1–15 (2021). https://doi.org/10.3390/pr9010157
37. Shaheen, A.; Sultana, S.; Lu, H.; Ahmad, M.; Asma, M.; Mahmood, T.: Assessing the potential of different nano-composite (MgO, $Al_2O_3$-CaO and $TiO_2$) for efficient conversion of Silybum eburneum seed oil to liquid biodiesel. J. Mol. Liq. **249**, 511–521 (2018). https://doi.org/10.1016/j.molliq.2017.11.053
38. Nouri, E.; Shahmiri, M.; Rezaie, H.R.; Talayian, F.: The effect of alumina content on the structural properties of $ZrO_2$-$Al_2O_3$ unstabilized composite nanopowders. Int. J. Ind. Chem. **3**, 1–8 (2012). https://doi.org/10.1186/2228-5547-3-17
39. Al-Fatesh, A.S.; Khatri, J.; Kumar, R.; Kumar Srivastava, V.; Osman, A.I.; AlGarni, T.S.; Ibrahim, A.A.; Abasaeed, A.E.; Fakeeha, A.H.; Rooney, D.W.: Role of Ca, Cr, Ga and Gd promotor over lanthana-zirconia–supported Ni catalyst towards $H_2$-rich syngas production through dry reforming of methane. Energy Sci. Eng. **10**, 866–880 (2022). https://doi.org/10.1002/ese3.1063
40. Al-Mubaddel, F.S.; Kumar, R.; Sofiu, M.L.; Frusteri, F.; Ibrahim, A.A.; Srivastava, V.K.; Kasim, S.O.; Fakeeha, A.H.; Abasaeed, A.E.; Osman, A.I.; Al-Fatesh, A.S.: Optimizing acido-basic profile of support in Ni supported $La_2O_3$+$Al_2O_3$ catalyst for dry reforming of methane. Int. J. Hydrog. Energy **46**, 14225–14235 (2021). https://doi.org/10.1016/j.ijhydene.2021.01.173
41. Du, X.; Wang, Y.; Su, X.; Li, J.: Influences of pH value on the microstructure and phase transformation of aluminum hydroxide. Powder Technol. **192**, 40–46 (2009). https://doi.org/10.1016/j.powtec.2008.11.008
42. Al-Fatesh, A.S.; Kumar, R.; Fakeeha, A.H.; Kasim, S.O.; Khatri, J.; Ibrahim, A.A.; Arasheed, R.; Alabdulsalam, M.; Lanre, M.S.; Osman, A.I.; Abasaeed, A.E.; Bagabas, A.: Promotional effect of magnesium oxide for a stable nickel-based catalyst in dry reforming of methane. Sci. Rep. **10**, 13861 (2020). https://doi.org/10.1038/s41598-020-70930-1
43. Al-Fatesh, A.S.; Patel, N.; Srivastava, V.; Osman, A.I.; Rooney, D.W.; Fakeeha, A.H.; Abasaeed, A.E.; Alotibi, M.F.; Kumar, R.: Iron-promoted zirconia-alumina supported Ni catalyst for highly efficient and cost-effective hydrogen production via dry reforming of methane. J. Environ. Sci. (2023). https://doi.org/10.1016/j.jes.2023.06.024
44. Fakeeha, A.H.; Vadodariya, D.; Alotibi, M.F.; Abu-Dahrieh, J.K.; Ibrahim, A.A.; Abasaeed, A.E.; Alarifi, N.; Kumar, R.; Al-Fatesh, A.S.: Pd +$Al_2O_3$-supported Ni–Co bimetallic catalyst for $h_2$ production through dry reforming of methane: effect of carbon deposition over active sites. Catalysts **13**, 1374 (2023). https://doi.org/10.3390/catal13101374
45. Chaudhary, M.L.; Al-Fatesh, A.S.; Kumar, R.; Lanre, M.S.; Frusteri, F.; AlReshaidan, S.B.; Ibrahim, A.A.; Abasaeed, A.E.; Fakeeha, A.H.: Promotional effect of addition of ceria over yttria-zirconia supported Ni based catalyst system for hydrogen production through dry reforming of methane. Int. J. Hydrog. Energy **47**, 20838–20850 (2022). https://doi.org/10.1016/j.ijhydene.2022.04.199
46. Ma, Y.; Yan, W.; Sun, Q.; Liu, X.: Raman and infrared spectroscopic quantification of the carbonate concentration in $K_2CO_3$ aqueous solutions with water as an internal standard. China Univ. Geosci. **12**, 1018–1030 (2021). https://doi.org/10.1016/j.gsf.2020.03.002
47. De La Pierre, M.; Carteret, C.; Maschio, L.; André, E.; Orlando, R.; Dovesi, R.: The Raman spectrum of $CaCO_3$ polymorphs calcite and aragonite: a combined experimental and computational study. J. Chem. Phys. **140**, 164509 (2014). https://doi.org/10.1063/1.4871900
48. Goula, M.A.; Charisiou, N.D.; Siakavelas, G.; Tzounis, L.; Tsiaoussis, I.; Panagiotopoulou, P.; Goula, G.; Yentekakis, I.V.: Syngas production via the biogas dry reforming reaction over Ni supported on zirconia modified with $CeO_2$ or $La_2O_3$ catalysts. Int. J. Hydrog. Energy **42**, 13724–13740 (2017). https://doi.org/10.1016/j.ijhydene.2016.11.196
49. Palla, M.; Kumar, S.; Li, Z.; Jockusch, S.; Russo, J.J.; Ju, J.; Bosco, F.G.; Rindzevicius, T.; Alstrom, T.S.; Schmidt, M.S.; Boisen, A.: Click chemistry based biomolecular conjugation monitoring using surface-enhanced Raman spectroscopy mapping. Proc. IEEE Sens. (2017). https://doi.org/10.1109/ICSENS.2016.7808595
50. Espinós, J.P.; Fernández, A.; González-Elipe, A.R.: Oxidation and diffusion processes in nickel–titanium oxide systems. Surf. Sci. **295**, 402–410 (1993). https://doi.org/10.1016/0039-6028(93)90287-T
51. Ruckenstein, E.; Lee, S.H.: Effect of the strong metal-support interactions on the behavior of model nickel/titania catalysts. J. Catal. **104**, 259–278 (1987). https://doi.org/10.1016/0021-9517(87)90358-7.10.1016/0021-9517(84)90381-6
52. Simoens, A.J.; Baker, T.K.; Dwyer, D.J.; Lund, C.R.F.; Madon, R.J.: A study of the nickel–titanium. J. Catal. **86**, 359–372 (1984). https://doi.org/10.1016/0021-9517(84)90381-6
53. Bayahia, H.; Fakeeha, A.H.; Al-Zahrani, S.A.; Alreshaidan, S.B.; Al-Awadi, A.S.; Alotibi, M.F.; Kumar, R.; Al-Fatesh, A.S.: $CO_x$ -free $H_2$ production via catalytic decomposition of $CH_4$ over Fe supported on tungsten oxide-activated carbon catalyst: effect of tungsten loading. Arab. J. Chem. **16**, 104781 (2023). https://doi.org/10.1016/j.arabjc.2023.104781
54. Chen, P.; Zhang, H.B.; Lin, G.D.; Hong, Q.; Tsai, K.R.: Growth of carbon nanotubes by catalytic decomposition of $CH_4$ or CO on a Ni-MgO catalyst. Carbon N. Y. **35**, 1495–1501 (1997). https://doi.org/10.1016/S0008-6223(97)00100-0
55. Charisiou, N.D.; Siakavelas, G.; Tzounis, L.; Sebastian, V.; Monzon, A.; Baker, M.A.; Hinder, S.J.; Polychronopoulou, K.; Yentekakis, I.V.; Goula, M.A.: An in depth investigation of deactivation through carbon formation during the biogas dry reforming reaction

for Ni supported on modified with $CeO_2$ and $La_2O_3$ zirconia catalysts. Int. J. Hydrog. Energy **43**, 18955–18976 (2018). https://doi.org/10.1016/j.ijhydene.2018.08.074
56. Kurdi, A.N.; Ibrahim, A.A.; Al-Fatesh, A.S.; Alquraini, A.A.; Abasaeed, A.E.; Fakeeha, A.H.: Hydrogen production from $CO_2$ reforming of methane using zirconia supported nickel catalyst. RSC Adv. **12**, 10846–10854 (2022). https://doi.org/10.1039/d2ra00789d
57. Aghamohammadi, S.; Haghighi, M.; Karimipour, S.: A comparative synthesis and physicochemical characterizations of Ni/$Al_2O_3$-MgO nanocatalyst via sequential impregnation and sol-gel methods used for $CO_2$ reforming of methane. J. Nanosci. Nanotechnol. **13**, 4872–4882 (2013). https://doi.org/10.1166/jnn.2013.7588
58. Kambolis, A.; Matralis, H.; Trovarelli, A.; Papadopoulou, C.: Ni/$CeO_2$-$ZrO_2$ catalysts for the dry reforming of methane. Appl. Catal. A Gen. **377**, 16–26 (2010). https://doi.org/10.1016/j.apcata.2010.01.013
59. Charisiou, N.D.; Baklavaridis, A.; Papadakis, V.G.; Goula, M.A.: Synthesis gas production via the biogas reforming reaction over Ni/MgO–$Al_2O_3$ and Ni/CaO–$Al_2O_3$ catalysts. Waste Biomass Valoriz. **7**, 725–736 (2016). https://doi.org/10.1007/s12649-016-9627-9
60. Kim, H.; Robertson, A.W.; Kwon, G.H.; Jang-Won, O.; Warner, J.H.; Kim, J.M.: Biomass-derived nickel phosphide nanoparticles as a robust catalyst for hydrogen production by catalytic decomposition of $C_2H_2$ or dry reforming of $CH_4$. ACS Appl. Energy Mater. **2**, 8649–8658 (2019). https://doi.org/10.1021/acsaem.9b01599
61. Damyanova, S.; Shtereva, I.; Pawelec, B.; Mihaylov, L.; Fierro, J.L.G.: Characterization of none and yttrium-modified Ni-based catalysts for dry reforming of methane. Appl. Catal. B Environ. **278**, 119335 (2020). https://doi.org/10.1016/j.apcatb.2020.119335
62. Rahemi, N.; Haghighi, M.; Babaluo, A.A.; Jafari, M.F.; Khorram, S.: Non-thermal plasma assisted synthesis and physicochemical characterizations of Co and Cu doped Ni/$Al_2O_3$ nanocatalysts used for dry reforming of methane. Int. J. Hydrog. Energy **38**, 16048–16061 (2013). https://doi.org/10.1016/j.ijhydene.2013.08.084
63. Khatri, J.; Al-fatesh, A.S.; Fakeeha, A.H.; Ibrahim, A.A.; Abasaeed, A.E.; Kasim, S.O.; Osman, A.I.; Patel, R.; Kumar, R.: Ce promoted lanthana-zirconia supported Ni catalyst system : a ternary redox system for hydrogen production. Mol. Catal. **504**, 111498 (2021). https://doi.org/10.1016/j.mcat.2021.111498
64. Hu, X.; Jia, X.; Zhang, X.; Liu, Y.; Liu, C.: jun: Improvement in the activity of Ni/$ZrO_2$ by cold plasma decomposition for dry reforming of methane. Catal. Commun. **128**, 105720 (2019). https://doi.org/10.1016/j.catcom.2019.105720
65. Pan, C.; Guo, Z.; Dai, H.; Ren, R.; Chu, W.: Anti-sintering mesoporous Ni–Pd bimetallic catalysts for hydrogen production via dry reforming of methane. Int. J. Hydrog. Energy **45**, 16133–16143 (2020). https://doi.org/10.1016/j.ijhydene.2020.04.066